

Evolution of cosmic superstring networks: a numerical simulation

Jon Urrestilla^{1,2} and Alexander Vilenkin²

¹*Department of Physics & Astronomy, University of Sussex, Brighton, BN1 9QH, United Kingdom*

²*Institute of Cosmology, Department of Physics and Astronomy, Tufts University, Medford, MA 02155, USA*

We study the formation and evolution of an interconnected string network in large-scale field-theory numerical simulations, both in flat spacetime and in expanding universe. The network consists of gauge $U(1)$ strings of two different kinds and their bound states, arising due to an attractive interaction potential. We find that the network shows no tendency to “freeze” and appears to approach a scaling regime, with all characteristic lengths growing linearly with time. Bound strings constitute only a small fraction of the total string length in the network.

I. INTRODUCTION

It has been recently realized [1] that fundamental strings and other string-like objects, such as D -strings, can have astronomical dimensions and play the role of cosmic strings.¹ Observing these objects in the sky would provide the most direct test of superstring theory. Both types of string are naturally formed in the course of brane-antibrane annihilation at the end of brane inflation [2, 3, 4, 5, 6]. Fundamental (F) and D -strings produced in the aftermath of this annihilation can form (p, q) bound states combining p F -strings and q D -strings. As a result the strings are expected to form an interconnected FD -network [5, 6], with different types of string joined in 3-way Y -type junctions.

Similar string networks can also be formed in field theory; a simple example has been recently given by Saffin [7]. His model includes two Abelian Higgs models, with an additional coupling between the Higgses. The model has a broken $U(1)_A \times U(1)_B$ symmetry, resulting in two types of string, and the coupling is chosen so that A and B -type strings are attracted to each other and can form (p, q) bound states. An even simpler example is the usual Abelian Higgs model. With a suitable choice of the Higgs and gauge couplings, corresponding to the type-I regime, this model allows stable strings with arbitrary windings, which can be joined in 3-way junctions [8]. Strings with extreme type I properties can also be formed in models with SUSY flat directions [9].

String networks with 3-way vertices can also arise in models with symmetry breaking of the kind $G \rightarrow Z_3$ [10], as well as in non-Abelian field theories with several types of strings corresponding to non-commuting symmetry generators [11, 12]. In the latter case, when two non-commuting strings cross, a third string starts stretching between them, resulting in two Y -junctions.

The evolution of cosmic string networks has been a subject of much recent discussion and debate.² Early work on Z_3 -strings [15], using a simple analytic model, suggested that at late times the characteristic scale of the network, $\xi = (\mu/\rho_s)^{1/2}$, exhibits scaling behaviour,

$$\xi(t) = \gamma t, \quad (1)$$

and

$$\rho_s/\rho \sim G\mu/\gamma^2. \quad (2)$$

Here, ρ_s and ρ are the average energy densities of the network and of the universe, respectively, μ is the string tension, and γ is a constant. A similar model was later used for Z_N networks having N strings joined at each vertex [16].

The magnitude of γ in Eq. (1) depends on the rate of energy loss by the network. In Z_3 models, the vertices can carry an unconfined magnetic charge. The energy of the network is then efficiently dissipated by gauge field radiation from these magnetic monopoles. Another energy loss mechanism is the formation of closed loops and of small nets disconnected from the main network. In the absence of magnetic charges, and if loop and net formation turn out to be inefficient, the remaining energy loss channel is the gravitational radiation. In this case, the analysis of [15] gives $\gamma \sim G\mu$, and Eq. (2) gives $\rho_s/\rho \sim 1/G\mu \gg 1$, indicating that the string network becomes so dense that it dominates the universe.

¹ Higher-dimensional D -branes with all but one dimension compactified will also appear as stringlike objects from a macroscopic point of view.

² One of the key questions is whether or not the network gets entangled and “freezes”, in which case it would eventually dominate the energy density of the universe [13, 14]. However, most recent work points to scaling evolution.

More sophisticated analytic models have recently been developed, aimed directly to describe cosmic superstrings. These models allow for several types of string with different tensions and use the velocity-dependent one-scale model of string evolution [17, 18] (see also [19]). The models make somewhat different assumptions about the physics of F - and D -string interaction. Tye, Wasserman and Wyman [17] assume that when F and D strings meet and “zip” to form a bound FD -string, the excess energy is released in the form of high-energy particles. If this picture is correct, it provides an important additional mechanism of energy loss by the network. They also assume that the entire network is characterized by a single length scale $\xi(t)$. Avgoustidis and Shellard [18] assume, on the other hand, that the energy released in the zipping process goes to increase the kinetic energy of strings, and thus remains in the network, and allow different length scales for different string types. Assuming that the rate of energy loss to loops from networks is about the same as that from “ordinary” strings, both models predict scaling evolution, with $\gamma \sim 1$, with energy about equally distributed between $(1, 0)$, $(0, 1)$, and $(1, \pm 1)$ strings, and with negligible amount of energy is higher- (p, q) strings.

Network evolution has also been studied in field-theory numerical simulations.³ Spergel and Pen [20] and later Copeland and Saffin [16] used a non-linear sigma-model to simulate non-commuting string networks. Hindmarsh and Saffin [21] performed a full field theory simulation of global Z_3 strings. In all this work, the network was found to scale with $\gamma \sim 0.1 - 1$, indicating efficient damping. The models used in [16, 20, 21] have some important differences from superstring networks. First, all types of string in these models have the same tension, while in an FD -network the tensions of all (p, q) strings are generally different. Second, the global symmetry breaking models used in [16, 20, 21] allowed for an additional energy loss mechanism – the radiation of massless Goldstone bosons – which is known to be rather efficient. On the other hand, superstring networks are expected to have only gravitational-strength couplings to massless (or light) bosons.⁴ Hence, there is a danger of string domination, unless the network can efficiently lose energy by loop or small net production.

A field theory simulation of an interconnected string network has been recently developed by Rajantie, Sakellariadou and Stoica [23]. They used a model of interacting scalar and gauge fields similar to the Saffin’s model [7], which allows two types of string and a spectrum of bound states. The dynamic range of their simulations was not sufficient to reach any conclusions about the statistical properties of the network and its scaling behaviour (or lack thereof). The main focus of Rajantie *et. al.* paper is on the effect of the long-range interaction induced by the Goldstone field in models where one of the two $U(1)$ symmetries of the model is global. They find that this interaction disrupts the string bound states in the network. This result is probably of little relevance for superstring FD -networks, since, as we already noted, superstring interactions are expected to have gravitational strength and thus have little effect on network dynamics.

In this paper, we have developed a new network simulation, which we believe to be closer to a “realistic” superstring network. We used a field theory model with two types of gauge strings and adopted Saffin’s [7] interaction potential to ensure that the strings form bound states. The details of the model and of the simulation are given in the next section. The results are presented in Section 3. Our conclusions are summarized and discussed in Section 4.

II. SIMULATION DETAILS

A. The model

Saffin’s model of interacting strings⁵ is defined by the Lagrangian [7]

$$\mathcal{L} = |D_\mu \phi|^2 + |D_\mu \psi|^2 - \frac{1}{4} F_{\mu\nu}^2 - \frac{1}{4} \mathcal{F}_{\mu\nu}^2 - V(|\phi|, |\psi|). \quad (3)$$

Here, ϕ and ψ are complex scalar fields, charged with respect to A_μ and B_μ gauge fields, respectively,

$$D_\mu = \partial_\mu - ieA_\mu, \quad \mathcal{D}_\mu = \partial_\mu - igB_\mu, \quad (4)$$

$$F_{\mu\nu} = \partial_\mu A_\nu - \partial_\nu A_\mu, \quad \mathcal{F}_{\mu\nu} = \partial_\mu B_\nu - \partial_\nu B_\mu, \quad (5)$$

³ Earlier simulations, using a simple model of straight strings joined at vertices, were performed in [15] for a Z_3 network and in [12] for non-Abelian strings.

⁴ The possibility of cosmic superstrings having stronger than gravitational couplings to massless Ramond-Ramond fields has been recently discussed by Firouzjahi [22].

⁵ Similar models have been studied in relation to composite defects [24, 25, 26, 27].

$$V(|\phi|, |\psi|) = \frac{\lambda_A}{4}(|\phi|^2 - \eta_A^2)^2 + \frac{\lambda_B}{4}(|\psi|^2 - \eta_B^2)^2 - \kappa(|\phi|^2 - \eta_A^2)(|\psi|^2 - \eta_B^2). \quad (6)$$

Without the last term in the potential, the model describes independent A - and B -strings. Bound states are formed if the parameter κ is chosen in the range [7]

$$0 < \kappa < \frac{1}{2}\sqrt{\lambda_A\lambda_B}. \quad (7)$$

In this paper we shall not attempt to explore the full parameter space of the model and consider only the special case where the strings are in the Bogomol'nyi limit,

$$\lambda_A = 2e^2, \quad \lambda_B = 2g^2. \quad (8)$$

We shall also set $e = g$ and $\eta_A = \eta_B$. With standard rescalings, the parameters of the model can then be reduced to

$$\eta_A = \eta_B = 1, \quad (9)$$

$$e = g = \frac{1}{2}\lambda_A = \frac{1}{2}\lambda_B = 1, \quad (10)$$

and the range of κ in Eq. (7) becomes

$$0 < \kappa < 1. \quad (11)$$

In most of our simulations we used the value $\kappa = 0.9$. Table I gives the corresponding string tensions, as well as the binding energies (per unit length of string), which are relatively large. We have also included in Table I the values for a larger $\kappa = 0.95$.

(m, n)	$\kappa = 0.90$		$\kappa = 0.95$	
	μ	$\Delta\mu$	μ	$\Delta\mu$
(1,0)	0.793	-	0.728	-
(1,1)	1.278	0.308	1.133	0.323
(2,1)	1.798	0.581	1.560	0.624

TABLE I: String tensions (μ) and bounding energies ($\Delta\mu$) for (m, n) type strings, calculated for $\kappa = 0.90$ [7] and $\kappa = 0.95$.

B. Numerical setup

Our aim was to perform real-time lattice simulations of model (3), for as long a time as our facilities allowed us. In order to do this, we obtained the equations of motions from (3),

$$\begin{aligned} \ddot{\phi} + 2\frac{\dot{a}}{a}\dot{\phi} - D_j D_j \phi &= -a^2 \phi \left[\frac{\lambda_A}{2} (|\phi|^2 - \eta_A^2) + \kappa (|\psi|^2 - \eta_B^2) \right] \\ \ddot{\psi} + 2\frac{\dot{a}}{a}\dot{\psi} - \mathcal{D}_j \mathcal{D}_j \psi &= -a^2 \psi \left[\frac{\lambda_B}{2} (|\psi|^2 - \eta_B^2) + \kappa (|\phi|^2 - \eta_A^2) \right] \\ \dot{F}_{0j} - \partial_i F_{ij} &= -2a^2 e \operatorname{Im}[\phi^* D_j \phi] \\ \dot{\mathcal{F}}_{0j} - \partial_i \mathcal{F}_{ij} &= -2a^2 g \operatorname{Im}[\psi^* \mathcal{D}_j \psi] \end{aligned} \quad (12)$$

where we have made a gauge choice $A_0 = B_0 = 0$ and assumed a flat FRW spacetime written in conformal time,

$$ds^2 = a^2(\tau)(d\tau^2 - d\mathbf{x}^2). \quad (13)$$

Overdots in Eqs. (12) stand for derivatives with respect to τ .

There is a well-known problem in such simulations: the string core has a fixed physical width, whereas the distance between lattice-points grows with the expansion ($a \propto \tau$ in radiation era, and $a \propto \tau^2$ in matter era). As a result the string width quickly drops below the resolution threshold of the simulation. Here, we have adopted the approach used

in [28, 29, 30, 31], in which the equations of motion are artificially modified to have the string width growing with the expansion, so as to be able to simulate them throughout the evolution.

Following [31], the equations of motion (12) can be written as:

$$\begin{aligned} \ddot{\phi} + 2\frac{\dot{a}}{a}\dot{\phi} - D_j D_j \phi &= -a^{2s} \phi \left[\frac{\lambda_A}{2} (|\phi|^2 - \eta_A^2) + \kappa (|\psi|^2 - \eta_B^2) \right] \\ \dot{F}_{0j} - 2(1-s)\frac{\dot{a}}{a}\partial_i F_{ij} &= -2a^{2s} e \mathcal{I}m[\phi^* D_j \phi] \end{aligned} \quad (14)$$

and likewise for ψ and B_μ . Here, s is a parameter that controls the growth of the string width, with $s = 1$ being the true value. As earlier work has shown [30, 31], there is little difference in string dynamics for different values of s . For the remainder of this work, we shall set $s = 0$ (that is, the string has constant comoving width).

We discretized the modified equations of motion (14) on a lattice using the standard lattice link variable approach [32] and performed the simulations on the UK National Cosmology Supercomputer [33]. The simulation box consisted of 512^3 lattice points, with periodic boundary conditions. We chose $\Delta x = 1.0$ and $\Delta \tau = 0.2$ trying to maximize the dynamical range of the simulation.

Scaling evolution regime is expected to be an attractor, and indeed earlier work has shown [31, 34, 35, 36] that this regime is approached from a wide range of initial configurations. Nonetheless, constructing initial conditions for this kind of simulation is a nontrivial task. The challenge is to find some initial configuration that leads to scaling as fast as possible, in order to maximize the dynamical range.

For the results presented here, we used the following procedure: we set all gauge fields and gauge field momenta to zero, also set the scalar field momenta to zero. The magnitudes of the scalar fields is set to η_A and η_B respectively (in the present work $\eta_A = \eta_B = 1$), and their phases are chosen randomly. This configuration was then smoothed out by averaging over nearest neighbours, and this procedure repeated 20 times, in order to get rid of some excess initial gradient energy. Note that this initial configuration satisfies the (lattice) Gauss law, and due to the lattice-link variable procedure, the Gauss law is guaranteed to be satisfied throughout the simulation.

The initial configuration described above corresponds to a highly excited state, so in order to remove the extra energy from the system, a fake constant damping was applied, $\gamma = \frac{\dot{a}}{a} = 0.2$, until time $\tau = 32$. From then on, we performed simulations for flat spacetime ($\gamma = 0$), radiation ($\gamma = 1/\tau$) and matter ($\gamma = 2/\tau$) eras. Only times $\tau > 64$ were used for this analysis.

In order to automatically detect the strings in the simulation and compute their length, we calculated the net winding of the phases around plaquettes. One can then trace the string following the winding and estimate the lengths. The length L of a string that crosses n plaquettes is estimated as $L = n \cdot \Delta x$.

An AB string can be traced by the sites where both A and B phases wind. Unfortunately, there are two drawbacks of this procedure: on the one hand, there are accidental crossings of A and B strings, i.e., lattice sites where an A string and a B string simply cross and follow their way, without any attempt to form a bound state. On the other hand, there are places where inside a clear segment of AB string, A and B phases do not wind in exactly the same plaquettes, but there is a slight displacement (we will show an example in the following Section). In order to circumvent these problems, we have excluded accidental crossing by setting a minimum size of AB string (l_{min}^{AB}), and also excluded gaps in AB segments (due to an occasional ‘‘displacement’’) shorter than a given distance (d_{max}^{AB}). This means that in the process of detecting AB segments, all segments of size $l < l_{min}^{AB}$ will not be considered as legitimate segments. Also, if the separation between two segments is $d < d_{max}^{AB}$, those two segments are considered as one. The total length of AB string is not considerably affected by this process; the main difference corresponds to a more realistic count of the number N of Y -junctions formed, that is, it helps in not overcounting AB -segments and Y -junctions. There is no obvious way of determining the values of l_{min}^{AB} and d_{max}^{AB} , and we have chosen them to be $l_{min}^{AB} = 3$ and $d_{max}^{AB} = 5$ by trial and error, and inspection of the results. With this choice, the corrected value of N is roughly a factor of 4 smaller than one would get from the raw data.

As we already mentioned, our choice of parameters was largely motivated by the effort to increase the dynamic range of the simulation. For example, we allocated only a few lattice points per string thickness. As a result, our discretized representation of the field theory string solutions is not particularly accurate. For a rapidly moving string, this may result in spurious damping, with the kinetic energy of the string being dissipated into particles [37]. Moore *et. al.* [30] performed numerical tests to determine the optimal choice of the lattice spacing Δx and concluded that $\Delta x = 0.5$ is close to the maximal value that still accurately represents the string dynamics. For larger values of Δx , they observed a significant increase in spurious particle emission from oscillating strings.

In the present paper, our focus is not so much on the dynamics of oscillating loops, as it is on the overall characteristics of the large network. In fact, in order to observe oscillating loops in field theory simulations Δx should be rather small (even smaller than 0.5), leaving us with a tiny dynamical range where large network properties would be impossible to study. We therefore pushed the parameter values a bit further and used $\Delta x = 1.0$, with the hope

that these properties will not be strongly affected. We performed several tests by simulating the system with different Δx ($0.5 < \Delta x < 1.0$), smoothness of the initial configuration (smoothing between 0 and 30 times), the value of the initial fake damping (between 0 and 0.5) and the length of time in which the fake damping was active ($0 < t < 50$). The qualitative results for all characteristic lengths of the network were the same in all cases, with the actual values agreeing within 10 – 20%. (The only exception is the length of A and B segments, as discussed in Sections III C and III D.)

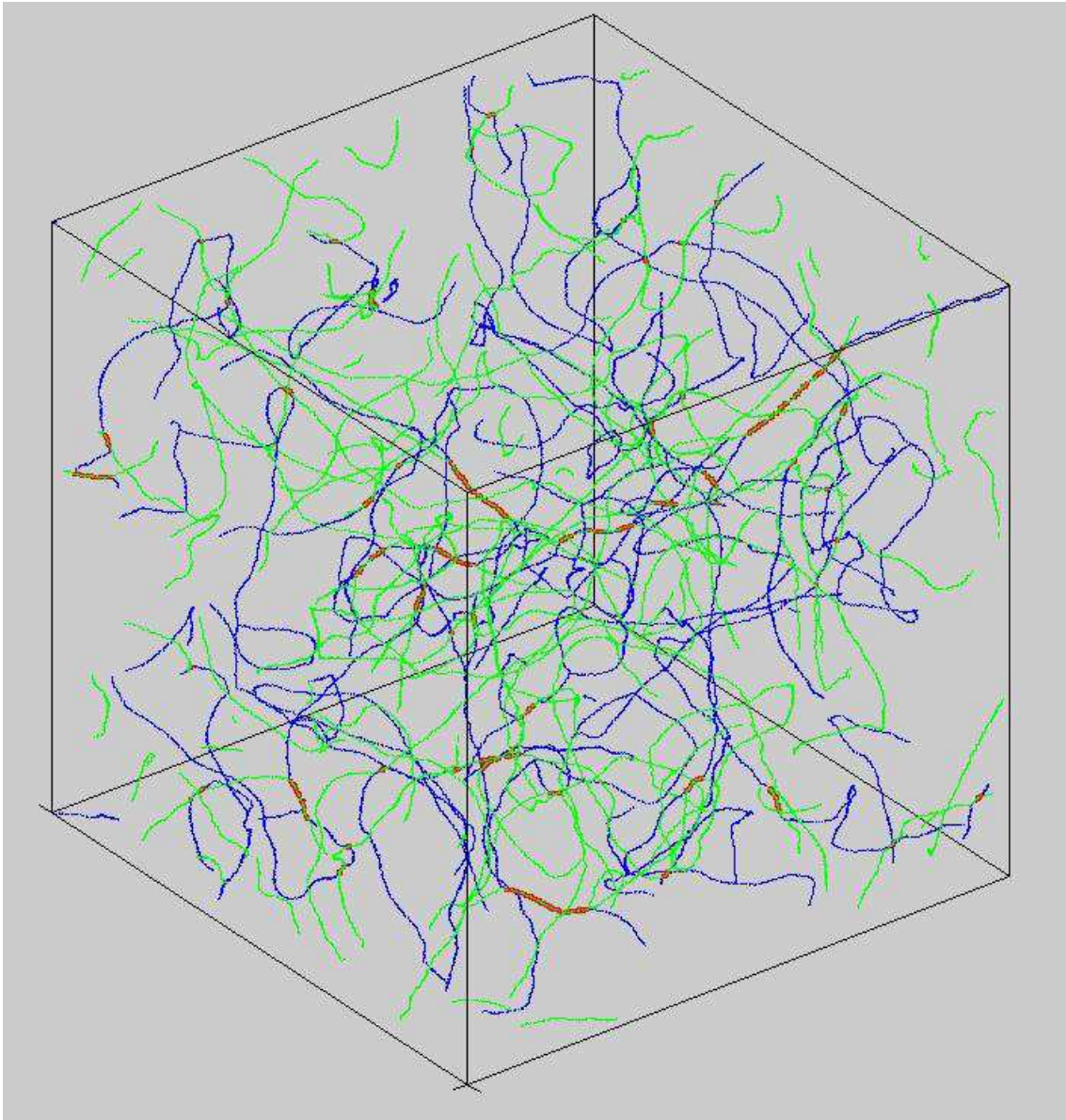


FIG. 1: Picture of a typical simulation of a (p,q) network. The green and blue colours correspond to A and B strings respectively, whereas the red colour shows the AB segments. It can be clearly seen how Y junctions are formed all over the simulation.

III. RESULTS

A. The network correlation scale ξ

Our simulations were performed in flat spacetime and in the radiation and matter eras. In all cases an interconnected network was formed with A -, B - and $(1,1)$ AB -strings. No higher- (p,q) strings were observed. A representative

snapshot of the network is shown in Fig. 1. Throughout the evolution, the network is dominated by one large (“infinite”) interconnected net, comprising more than 90% of the total string length, as seen in Fig. 2.

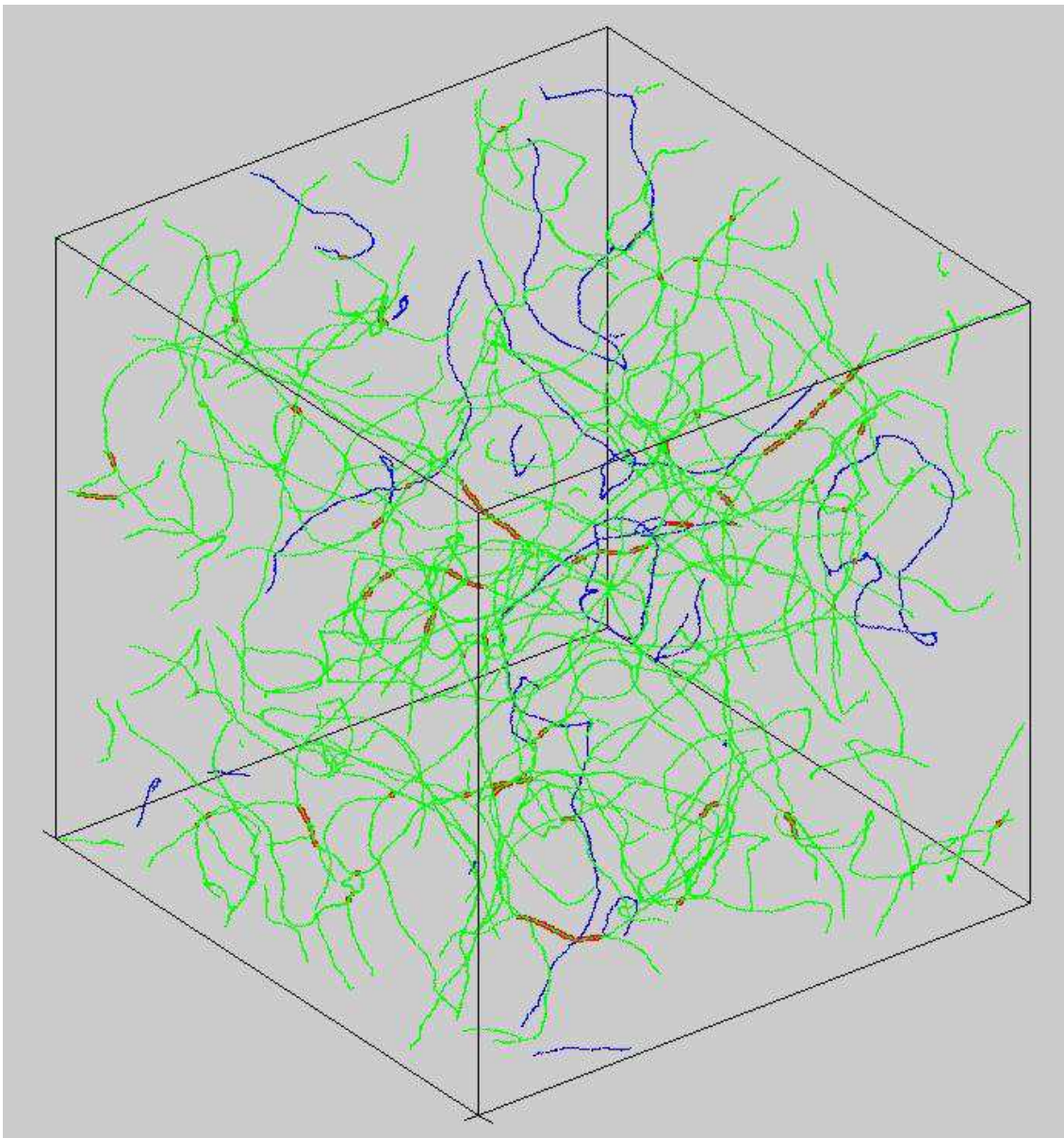


FIG. 2: Picture of a typical simulation of a (p,q) network. This picture represents the same configuration, but we show how most of the string length (typically more than 90%) forms an interconnected network (A and B strings in the main network shown in green and AB segments in red) and there are only a few loops that do not belong to the main network (blue).

As mentioned in the previous section, within a single AB bound state, A and B strings can be displaced by a single lattice point, making the code decide that it is in fact two separate segments. Figure 3 shows a fragment of the simulation box, with a somewhat long AB string depicted. Those accidental displacements should not be taken into account, and with the help of the parameter d_{max}^{AB} (introduced earlier), the displacements are reassessed, and the segment is counted as one.

The overall length scale of the network can be defined as usual,

$$\xi = (V/L)^{1/2}, \quad (15)$$

where V is the volume of the simulation box, L is the total length of string,

$$L = L_A + L_B + L_{AB}, \quad (16)$$

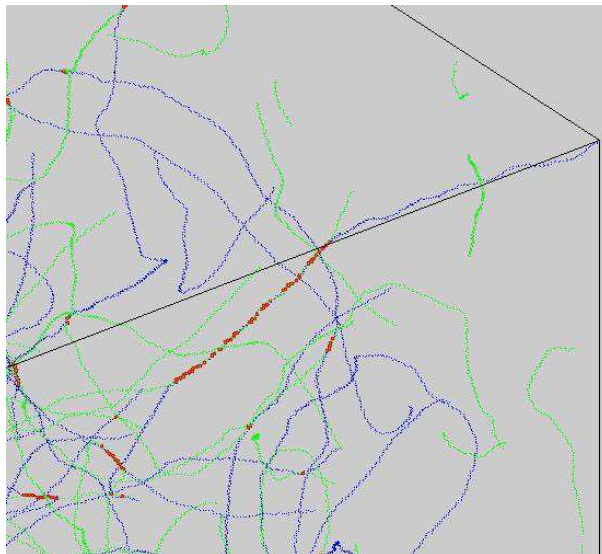


FIG. 3: Fragment of the simulation box showed in Fig. 1. Green and blue correspond to A and B string, whereas the red colour corresponds to an AB segment. A long AB segment can be seen in the picture, but at some points the A and B string miss each other by just a lattice point. With the help of the parameter d_{max}^{AB} those accidental displacements are accounted for, and long segments such as the one in the figure are counted as one.

and L_A , L_B and L_{AB} are the lengths in A , B and AB strings, respectively. ξ gives the typical distance between strings in the network.

Throughout this paper we shall use *comoving* length scales. The corresponding physical lengths, which will be denoted by superscript (ph), can be obtained by multiplying with the scale factor $a(\tau)$, e.g.,

$$\xi^{(ph)}(\tau) = a(\tau)\xi(\tau). \quad (17)$$

For our models, the scale factor has the form

$$a(\tau) = (\tau/\tau_0)^n, \quad (18)$$

with $\tau_0 = const$ and $n = 0, 1, 2$ for flat spacetime, radiation and matter eras, respectively. The physical time t and the horizon distance ℓ_H are given by

$$t = \int_0^\tau a(\tau')d\tau' = \frac{\tau^{n+1}}{(n+1)\tau_0^n}, \quad (19)$$

$$\ell_H = a(\tau)\tau = (n+1)t. \quad (20)$$

The simulation results for $\xi(\tau)$ are shown in Fig. 4, where each graph represents an average over 10 simulations. Remarkably, the graphs for the flat, radiation and matter regimes are almost identical. They show a nearly linear dependence,

$$\xi(\tau) = \alpha\tau + \xi^{(0)}, \quad (21)$$

with $\alpha \approx 0.15$ (see Table II). Toward the end of the simulation, the two terms in Eq. (21) are comparable to one another. If the linear dependence extends to much larger values of τ , the constant term eventually becomes negligible,

$$\xi \approx \alpha\tau, \quad (22)$$

and the corresponding physical length grows proportionally to the horizon,

$$\xi^{(ph)}(t) \approx (n+1)\alpha t = \alpha\ell_H(t). \quad (23)$$

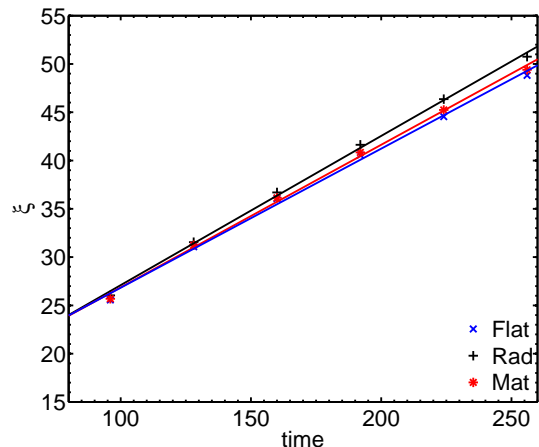


FIG. 4: The correlation length ξ , as defined in Eqn. 15, averaged over 10 simulations for flat (dashed black), radiation (continuous red) and matter (dotted blue) regimes. Note that all three cases exhibit an approximately linear behaviour, nearly independent of the regime.

	Flat	Radiation	Matter
$\alpha (\xi)$	0.14	0.15	0.15
$\alpha_A (\xi_A)$	0.21	0.22	0.21
$\alpha_{AB} (l_{AB})$	0.03	0.07	0.08
$\alpha_N (\xi_N)$	0.21	0.28	0.30

TABLE II: The values of the linear growth coefficients of different lengths, as defined in the body of the paper, obtained by fitting the simulation data. Note that with our parameter values $\alpha_A = \alpha_B$.

B. Bound strings

An important characteristic of the network is the fraction of total string length in bound (AB) strings,

$$f_{AB} = \frac{L_{AB}}{L_A + L_B + L_{AB}}. \quad (24)$$

The simulation results for f_{AB} are shown in Fig. 5. We see that f_{AB} remains nearly constant, at the value $0.01 \leq f_{AB} \leq 0.02$ in radiation and matter eras, and somewhat lower for flat spacetime. Hence, bound strings constitute less than 2% of the network. This is in conflict with analytic models [17, 18] predicting that the energy of the network should be more or less equally divided between A , B and AB -strings. The main source of the discrepancy is the assumption made in [17, 18] that crossings of A and B strings typically lead to the formation of relatively stable bound AB segments of length $\sim \xi(t)$. Visual inspection of the simulation movies suggests, on the contrary, that formation of bound segments by intersecting A and B strings occurs rather infrequently, probably when the relative velocity of the colliding strings is sufficiently small [38, 39]. Even when they are formed, the AB -segments easily “unzip” as the free A and B ends pull in different directions and do not usually last for more than a Hubble time.

Even though the fraction of bound string is small, the interaction of A and B -strings has a significant effect on the network evolution. To quantify this effect, we ran some simulations with the same initial conditions for A -string fields as before, but with B -string fields starting in their ground state, so that no B strings are formed. A -strings then evolve as ordinary $U(1)$ strings, and their characteristic length

$$\xi_A = (V/L_A)^{1/2} \quad (25)$$

exhibits a linear dependence on τ with $\alpha_A \approx 0.29$, as seen in Fig. 6. (This value is in agreement with earlier $U(1)$ simulations by Vincent et. al. [40] and Moore et. al. [30].) The same quantity calculated with B -strings present gives $\alpha_A \approx 0.22$, so the growth of ξ_A is significantly slower than it would be if the two kinds of string evolved independently.

The average (comoving) length of AB -segments is

$$l_{AB} = L_{AB}/N, \quad (26)$$

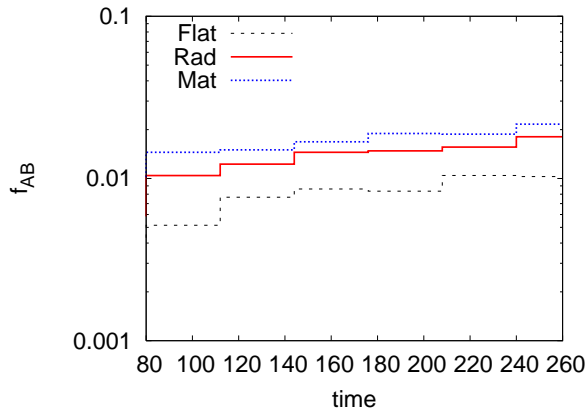


FIG. 5: Fraction of total string length in bound strings, for flat, radiation and matter regimes. The percentage is fairly low; between 0.5-1% for flat, and 1-2% for radiation and matter cases.

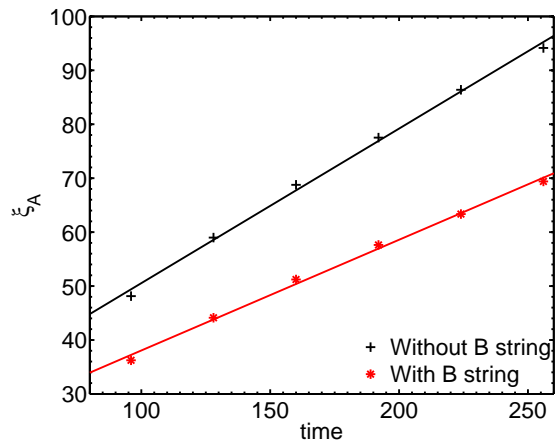


FIG. 6: Comparison of ξ_A (only in radiation era, for clarity) between simulations points and without B -strings.

where N is the number of AB -segments ($2N$ is the number of Y -junctions where the three types of string meet). Fig. 7 shows that the evolution of l_{AB} is approximately linear,

$$l_{AB} \approx \alpha_{AB}\tau + l_{AB}^{(0)}. \quad (27)$$

The coefficient α_{AB} (see Table II) is nearly the same in radiation and matter eras (within 10%), $\alpha_{AB}^{(rad,mat)} \approx 0.07$, and is significantly smaller in flat spacetime, $\alpha_{AB}^{(flat)} \approx 0.025$. The shorter bound segments in flat spacetime are probably due to larger string velocities.

The typical distance between Y -junctions is given by

$$\xi_N = (V/2N)^{1/3}. \quad (28)$$

Once again, we find approximately linear evolution (see Fig. 8),

$$\xi_N \approx \alpha_N\tau + \xi_N^{(0)}, \quad (29)$$

with $\alpha_N \approx 0.3$.

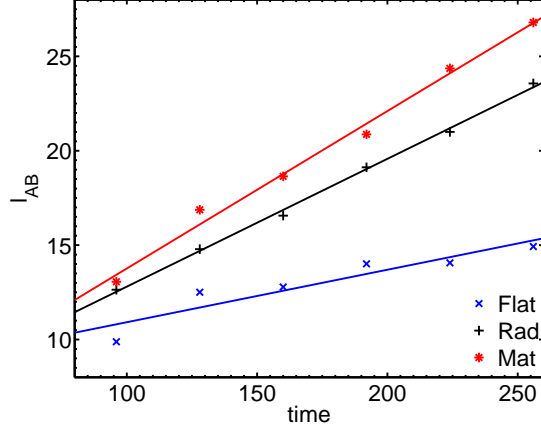


FIG. 7: The average length of bound segments l_{AB} , as defined in Eq. 26, for flat, radiation and matter regimes. The evolution is approximately linear, with slope given in Table II.

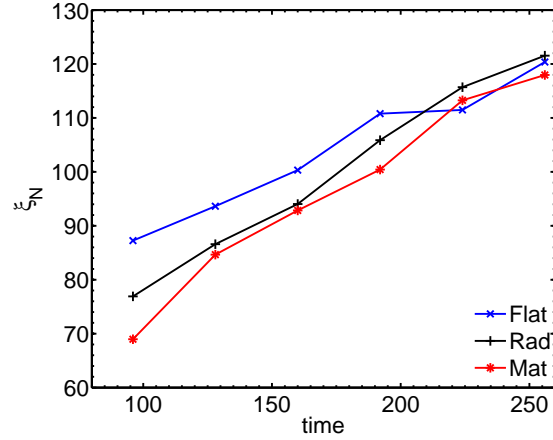


FIG. 8: The average distance between Y-junctions, ξ_N as defined in Eq. 28, for flat, radiation and matter regimes. The evolution is approximately linear, with slope given in Table II.

C. Non-scaling of A and B segments

All results presented so far are consistent with scaling evolution, with all characteristic length scales of the network growing proportionally to the horizon. However, the average comoving lengths of A and B segments,

$$l_A = L_A/N, \quad l_B = L_B/N, \quad (30)$$

do not exhibit scaling behaviour. In fact, Fig. 9 shows that, rather surprisingly, these lengths approach nearly constant values,

$$l_A \approx l_B \approx \text{const.} \quad (31)$$

The corresponding physical lengths grow proportionally to the scale factor.

Throughout the simulation, the segment length l_A remains much greater than the correlation length ξ_A . The correlation length grows with time, but is still about an order of magnitude smaller than l_A at the end of the simulation (and similarly for l_B and ξ_B). This suggests that A (and B) segments have the shape of random walks of step $\sim \xi_A$ and end-to-end distance $\sim \xi_N$. The length of the segments is then

$$l_A \sim \xi_N^2/\xi_A. \quad (32)$$

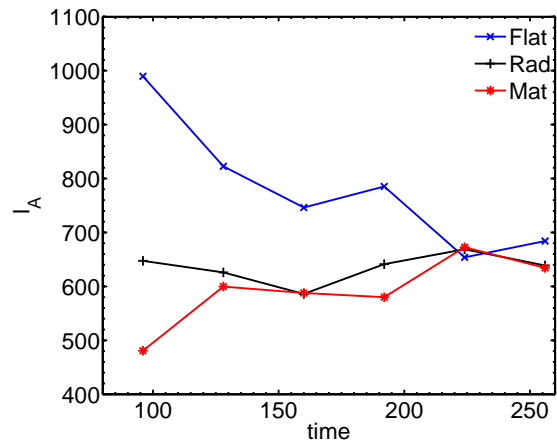


FIG. 9: The average length of A -segments l_A is shown for flat, radiation and matter regimes. In all three cases, l_A is nearly constant at late times. The behaviour of l_B is essentially the same.

Physical time	Damping (γ)	Δt
$0 < t < 32$	0.5	0.2
$32 < t < 272$	2.0	0.5
$t > 272$	$2.0/t$ (rad.)	0.2

TABLE III: Values of the parameters in simulation with a second damping period, introduced to achieve scaling of the segment lengths l_A and l_B .

We have verified that the ratio $\xi_N^2/\xi_A l_A = \xi_A/2\xi_N$ is indeed approximately a constant of order 0.3, within 10 – 20%.

If the length of the segments l_A continues to grow slower than their end-to-end distance ξ_N , the two lengths will eventually become comparable to one another, with segments becoming more or less straight. This could mark the beginning of the true scaling regime, where all the characteristic lengths of the network have the same order of magnitude and grow proportionally to τ . In any case, the evolution laws (21),(27),(31) cannot continue indefinitely and must stop at some $\tau = \tau_*$. The situation here may be somewhat similar to that with “ordinary” (not interconnected) strings, where scaling of the characteristic length $\xi(t)$ is quickly established, but scaling of the small wiggles on long strings and of closed loops is reached only after a long transient period [41, 42, 43, 44]. We shall refer to the evolution at $\tau < \tau_*$ as the transient scaling regime.

D. Towards a true scaling regime

We attempted to shorten this transient regime, or avoid it altogether, by increasing the duration of the initial damped period. This has the effect of increasing N and decreasing the ratio $l_A/\xi_N \sim (\xi_N/\xi_A)^2$ in the initial state (right after damping is turned off). Getting to the end of the transient regime by the end of the simulation proved to be a difficult task, for which we had to push the limits of the stability of the code by using a rather large time step, a rather large damping coefficient, and evolving the system beyond the half-light-crossing time of the simulation box.

We performed a set of 20 simulations with the values of time step Δt and the damping parameter γ shown in Table III. The difference from the rest of our simulations is in the second period of damping imposed after the first period (which is common to all simulations and is used to relax the system from the highly excited initial state and allow string formation). The extra damping period has a time-discretization of $\Delta t = 0.5$ (keeping $\Delta x = 1$), and the numerical stability is achieved because the damping is also rather high ($\gamma = 2.0$).

Figure 10 shows the length measures ξ_A , ξ_N , l_A averaged over the 20 simulations. All three lines seem to approach a linear behaviour. The slopes of ξ_A and ξ_N agree with the ones obtained earlier, without an extended damping period. Other quantities characterizing the system, such as α_{AB} , f_{AB} and the percentage of string length in loops, also agreed with the ones for the simulations without extra damping. The fairly linear behaviour of l_A is the main change. A linear fit to the evolution of l_A gives

$$l_A \approx \alpha_{LA}\tau + l_A^{(0)}, \quad (33)$$

with $\alpha_{LA} \approx 0.8$. Extrapolating this behaviour to large τ , we expect a scaling regime in which l_A is a few times larger than ξ and ξ_N . However, because of our extreme choice of parameters and large error bars in l_A , and because the change in l_A during the linear regime is relatively small, this conclusion should be regarded as tentative.

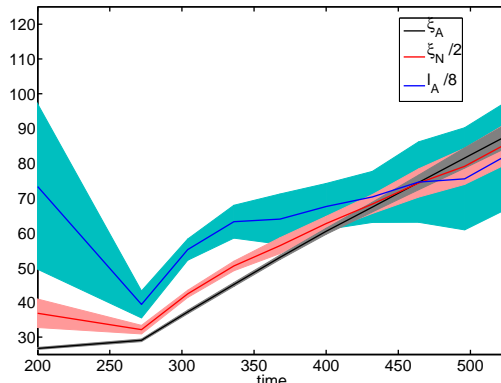


FIG. 10: The length measures ξ_A , ξ_N , l_A averaged over 20 simulations performed with an extended damping period, as explained in Section III C. The thick lines corresponds to the average, whereas the shaded regions correspond to $1\text{-}\sigma$ statistical errors over the simulations.

E. Loops and small nets

We observed the formation of small independent nets a few times in the course of the simulation, but these occasions were rather rare, so AB -strings belonged predominantly to the infinite network, with at most one small net in addition. The fraction of the total string length in disconnected A - or B -loops is shown in Fig. 11. We see that this fraction remains nearly constant, at a value $f_L \sim 0.03 - 0.05$ in radiation and matter eras and $f_L \sim 0.08$ in flat spacetime.

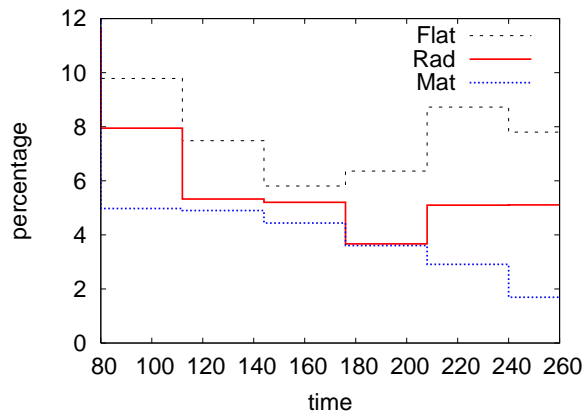


FIG. 11: Percentage of string length for both A and B strings in loops that do not belong to the main network.

The length distribution of independent loops is plotted in Fig. 12, averaged over 20 simulations in radiation era. The figure uses logarithmic binning and shows the distribution of loops at four different times. We see that some of the loops are fairly large, with length much greater than the inter-string separation ξ . Such loops should arguably be regarded as part of the infinite network. Indeed, if the diameter of a loop is larger than a few times ξ_A (or ξ_B) for a given time, the loop is very likely to reconnect to the network. If we exclude loops longer than $6\xi_A$ ($3\xi_A$), the percentage of string length in loops drops to $1 - 2\%$ (0.5%). These values are in agreement with previous field theoretical simulations where a loops were found to account for a few percent of the total string length [40].

Simulation movies show that loops that decouple from the network do not oscillate as they would in Nambu-Goto simulations, but rather shrink and disintegrate. This could be expected, since it is well known that in order to observe

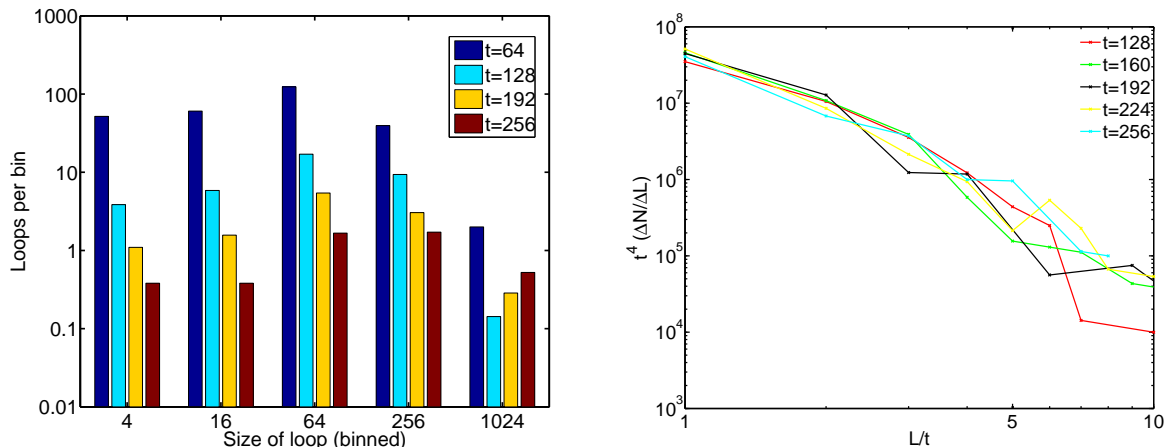


FIG. 12: (Left) Distribution of independent loops for the radiation era, averaged over 20 simulations, for four different time steps. The figure shows that there are rather large independent loops formed during the simulation, and that the peak of the distribution tends to move towards larger sizes with time. (Right) Loop distribution averaged over 20 simulations in radiation era. The distribution appears to follow Eqn. 34 rather well, suggesting that it is scaling.

oscillating loops in field theory simulations one would need very large loops and very small values of the lattice spacing. Additional damping, through particle emission from loops, may be due to the presence of short-wavelength string excitations in the initial conditions, as indicated by the numerical results of Refs. [45, 46]. The short lifetimes of the loops in our simulations explain, at least in part, the relatively small amount of string in loops, as compared to the Nambu-Goto simulations.

In any case, we checked the loop distribution in our simulations for scaling behavior. On dimensional grounds, the number density of loops per unit length interval in a scaling network should have the form

$$\frac{dn}{dl}(t) = t^{-4} f(l/t). \quad (34)$$

Defining ΔN_i as the number of loops between sizes l_i and l_{i+1} and $\Delta l_i = l_{i+1} - l_i$, we plot in Fig. 12 the (binned) quantity $\frac{\Delta N_i}{\Delta l_i} t^4$, obtained for 5 different times and averaged over 20 simulations. In a situation where the loop distribution scales, all the lines should line on top of one another. We see that the graph in Fig. 12 does indeed exhibit scaling.

F. Effect of higher binding energy

We ran some simulations with a greater value of the string binding parameter, $\kappa = 0.95$, in order to try to understand how sensitive our results were to the precise value of κ . The main difference encountered in these simulations was the fraction of bound string f_{AB} increased by a factor ~ 1.5 (see Fig. 13). Our analysis showed that the effect on the correlation lengths ξ and on the loop distribution was very small. Actually, the values of the coefficient of the different length measures were the same as in the $\kappa = 0.9$ case, the only difference being a smaller α_N for this case (0.16, 0.22, 0.25 for flat, radiation and matter eras, respectively).

IV. CONCLUSIONS AND DISCUSSION

We performed numerical simulations of the formation and evolution of string networks using the Saffin's model for interacting strings. The model has two types of Abelian gauge strings, A and B , with an attractive interaction which gives rise to bound AB -strings. Starting with a randomized high-energy field distribution, we found that an interconnected string network is indeed formed, consisting of A and B strings, as well as their $(1, 1)$ bound states, joined together at Y -type junctions. No higher (p, q) -strings were observed in the simulations.

Throughout each simulation, the network is dominated by a single ("infinite") net, with occasional small nets and a fair number of disconnected closed loops being formed in the course of the evolution. The characteristic length scale

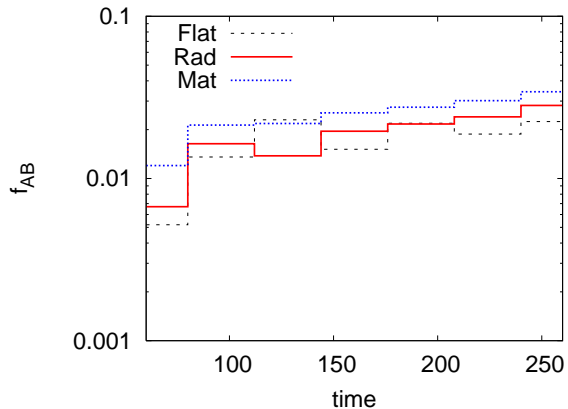


FIG. 13: Fraction of total string length in bound strings, for flat, radiation and matter regimes, for simulations with $\kappa = 0.95$. The percentage is still fairly low, though somewhat higher than for $\kappa = 0.90$ (Fig. 5)

of the network approaches the scaling regime where it grows proportionally to time, $\xi(\tau) = \alpha\tau$ with $\alpha \sim 0.15$, in both radiation and matter eras, as well as in flat spacetime. Other characteristic length scales, such as the length of AB segments, the typical correlation length of A and B strings or the typical distance between Y junctions also scale.

A surprising feature of our simulation is that bound AB -strings constitute only a small fraction of the total string length ($\sim 2\%$). Also, the average length of AB -segments is much shorter than the length of A - or B -string segments. This is in contrast with analytic models [17, 18] predicting all lengths to be fairly equal. From movies of the simulations one can see that AB -segments do not always form when an A -string meets a B -string (even for relatively high bounding energies); on the contrary, the formation of bound segments is rather infrequent. Even though new AB -segments are constantly formed, their lifetime is relatively short, usually less than the Hubble time, as the segments are “unzipped” by the free A and B ends pull them in different directions.

Even though, with our general initial condition configuration, most of the typical distances in the network showed a scaling behaviour, the average comoving lengths of A and B segments did not. These lengths remained much larger than the typical correlation length throughout the simulation. This evolution regime cannot continue indefinitely, since the correlation length ξ would eventually catch up with the segment lengths l_A and l_B . In an attempt to go beyond this transient regime and reach true scaling, we introduced an extra period of strong damping at early times (which has the effect of decreasing l_A/ξ) and pushed the parameters to extend the dynamic range of the simulation. We found that the system does seem to approach a regime where all characteristic lengths scale linearly with time. If this were the true scaling regime, it would provide us, among other things, with the means to calculate CMB power spectra predictions from the field theoretical model as in [31, 47, 48, 49]. But due to a relatively short duration of the linear evolution and to likely presence of spurious damping, our simulations cannot be relied upon for a quantitatively accurate description of scaling.

Disconnected closed loops constitute about 10% of the total string length. Some of these loops are very large and will very likely reconnect into the main network again. If one factors out disconnected loops of length larger than a few times the correlation length, the total string length in loops drops to below 2%, in agreement with [40]. We examined the length distribution of loops in the network and found that, even though our parameter choice is not expected to resolve accurately string dynamics, these distributions seem to scale.

The network properties in our simulations are closer to those of superstring networks than they were in earlier simulations that used Z_3 -strings or non-linear sigma-models. However, there is still an important difference. On the one hand, our A and B strings have the same tension, as opposed to F - and D - strings. On the other, collision of same-type strings in our model always result in reconnection (unless the string segments are moving extremely fast [50]), while in the case of superstrings the reconnection probability is $p < 1$ and can even be small [4, 5, 51]. This feature can be accounted for in Nambu-Goto and analytic models.

The efficiency of various energy loss mechanisms by the string network remains a topic for future research. Energy loss to loop production appears to be substantial, considering that the length in loops at any time is a few percent of the total and that the loops do not stay around for long and rapidly decay. Another important energy loss mechanism in field theory simulations is direct particle emission from strings [40, 52]. In fact, the analysis in [18] shows that emission of particles and of tiny loops which immediately decay into particles is the dominant energy loss mechanism for a single $U(1)$ string network, so it probably dominates in our simulations as well. It has been argued in [18, 45, 46] that this effect is spurious and is due partly to insufficient resolution of the simulations and partly to excessive

amount of noise in the initial conditions. This issue is not completely settled, since some of the recent Nambu-Goto simulations [43] and analytic treatments [53] indicate continuous production of microscopic loops throughout the network evolution.

In summary, what have we learnt from our simulations? We have demonstrated that an interconnected network of strings can indeed form at a symmetry breaking phase transition. This network shows no tendency to freeze to a static configuration. On the contrary, it appears to approach scaling, with all characteristic lengths growing linearly with time. Qualitatively, our results indicate that bound strings constitute only a small part of the total string length and that the A and B string segments are rather wiggly, having lengths significantly greater than the correlation length ξ . The latter property leads to relatively frequent self-intersections and allows the network to lose a substantial fraction of its energy in the form of closed loops. Our simulations also indicate that the true scaling evolution may be preceded by a transient regime in which the comoving lengths of A and B -segments remain nearly constant in time.

Some of the shortcomings of our approach can be overcome in Nambu-Goto-type simulations (e.g., of the kind developed in [54]) or in analytic models (along the lines of [17, 18]). Either of these approaches, however, requires some microphysical input. For example, one needs to know under what conditions a bound string is formed in a string collision, what fraction of the binding energy of the newly formed string is radiated away, etc. The advantage of a direct field theory simulation is that it accurately represents the microphysics. A combination of all three approaches will probably be needed to reach a full understanding of network evolution.

V. ACKNOWLEDGEMENTS

We would like to thank José Juan Blanco-Pillado, Mark Hindmarsh, Andrew R. Liddle, Ken Olum and Vitaly Vanchurin for useful discussions. This work was supported by the US National Science Foundation (JU and AV), by Marie Curie Intra-European Fellowship MFIT-CT-2005-009628 and FPA2005-04823 (JU). This work has also been supported by the Spanish Consolider-Ingenio 2010 Programme CPAN (CSD2007-00042). The simulations were performed on cosmos, the UK National Cosmology Supercomputer, supported by SGI, Intel, HEFCE and PPARC.

-
- [1] For recent reviews, see J. Polchinski, Introduction to cosmic F - and D -strings, arXiv:hep-th/0412244; A.C. Davis and T.W.B. Kibble, *Contemp. Phys.* **46**, 313 (2005).
 - [2] M. Majumdar and A. Christine-Davis, *JHEP* **0203**, 056 (2002).
 - [3] S. Sarangi and S.H. Tye, *Phys. Lett.* **B536**, 185 (2002).
 - [4] N.T. Jones, H. Stoica and S.H. Tye, *Phys. Lett.* **B563**, 6 (2003).
 - [5] G. Dvali and A. Vilenkin, *JCAP* **0403**, 010 (2004).
 - [6] E.J. Copeland, R.C. Myers and J. Polchinski, *JHEP* **0406**, 013 (2004).
 - [7] P.M. Saffin, *JHEP* **09**, 011 (2005).
 - [8] M. Donaire and A. Rajantie, *Phys. Rev.* **D73**, 063517 (2006).
 - [9] Y. Cui, S.P. Martin, D.E. Morrissey and J.D. Wells, arXiv:0709.0950 [hep-ph].
 - [10] M. Aryal, A.E. Everett, A. Vilenkin and T. Vachaspati, *Phys. Rev.* **D34**, 434 (1986).
 - [11] T.W.B. Kibble, *J. Phys.* **A9**, 1387 (1976).
 - [12] P. McGraw, *Phys. Rev.* **D57**, 3317 (1998).
 - [13] A. Vilenkin, *Phys. Rev. Lett.* **53**, 1016 (1984).
 - [14] M. Bucher and D.N. Spergel, *Phys. Rev.* **D60**, 043505 (1999).
 - [15] T. Vachaspati and A. Vilenkin, *Phys. Rev.* **D35**, 1131 (1987).
 - [16] E.J. Copeland and P.M. Saffin, *JHEP* **0511**, 023 (2005).
 - [17] S.-H. Tye, I. Wasserman and M. Wyman, *Phys. Rev.* **D71**, 103508 (2005).
 - [18] A. Avgoustidis and E.P.S. Shellard, arXiv: astro-ph/0705.3395.
 - [19] C.J.A.P. Martins, *Phys. Rev.* **D70**, 107302 (2004).
 - [20] D. Spergel and U.-L. Pen, *Ap.J.* **491**, L67 (1997).
 - [21] M. Hindmarsh and P.M. Saffin, *JHEP* **0686**, 066 (2006).
 - [22] H. Firouzjahi, arXiv:hep-th/0710.4609.
 - [23] A. Rajantie, M. Sakellariadou and H. Stoica, arXiv:0706.3662 [hep-th]
 - [24] E.R. Bezerra de Mello, Y. Brihaye and B. Hartmann, *Phys. Rev.* **D67**, 045015 (2003)
 - [25] A. Achúcarro and J. Urrestilla, *Phys. Rev.* **D68**, 088701 (2003)
 - [26] E.R. Bezerra de Mello, *Phys. Rev.* **D68**, 088702 (2003)
 - [27] A. Achúcarro, B. Hartmann and J. Urrestilla, *JHEP* **0507**, 006 (2005)
 - [28] W.H. Press, B.S. Ryden and D.N. Spergel, *Ap. J.* **347**, 590 (1989)
 - [29] B.S. Ryden, W.H. Press and D.N. Spergel, *Ap. J.* **357**, 293 (1990)
 - [30] J.N. Moore, E.P.S. Shellard and C.J.A.P. Martins, *Phys. Rev.* **D65**, 023503 (2001).

- [31] N. Bevis, M. Hindmarsh, M. Kunz and J. Urrestilla, Phys. Rev. **D75**, 065015 (2007)
- [32] K.J.M. Moriarty, E. Myers and C. Rebbi, Phys. Lett. **B207**, 411 (1998)
- [33] UK National Cosmology Supercomputer: SGI Altix 3700 containing 152×1.3 GHz Intel Itanium II CPUs, www.damtp.cam.ac.uk/cosmos/
- [34] J. Urrestilla, A. Achúcarro, J. Borrill, A.R. Liddle, JHEP **0208**, 033 (2002)
- [35] M. Pickles and J. Urrestilla, JHEP **0301**, 052 (2003);
- [36] A. Achúcarro, P. Salmi and J. Urrestilla, Phys. Rev. **D75**, 121703 (2007)
- [37] J.J. Blanco-Pillado and K.D. Olum, private communication.
- [38] E.J. Copeland, T.W.B. Kibble, D.A. Steer, Phys. Rev. Lett. **97**, 021602 (2006)
- [39] E.J. Copeland, H. Firouzjahi, T.W.B. Kibble and D.A. Steer, arXiv:0712.0808 [hep-th].
- [40] G. Vincent, N. D. Antunes, M. Hindmarsh, Phys. Rev. Lett. **80**, 2277 (1998)
- [41] V. Vanchurin, K.D. Olum and A. Vilenkin, Phys. Rev. **D74**, 063527 (2006).
- [42] C.J.A.P. Martins and E.P.S. Shellard, Phys. Rev. **D73**, 043515 (2006).
- [43] C. Ringeval, M. Sakellariadou and F. Bouchet, JCAP **0702**, 023 (2007).
- [44] K.D. Olum and V. Vanchurin, Phys. Rev. **D75**, 063521 (2007).
- [45] J.N. Moore and E.P.S. Shellard, arXiv:hep-ph/9808336.
- [46] K.D. Olum and J.J. Blanco-Pillado, Phys. Rev. Lett. **84**, 4288 (2000).
- [47] N. Bevis, M. Hindmarsh, M. Kunz and J. Urrestilla, arXiv:astro-ph/0702223.
- [48] N. Bevis, M. Hindmarsh, M. Kunz and J. Urrestilla, Phys. Rev. **D76**, 043005 (2007)
- [49] J. Urrestilla, N. Bevis, M. Hindmarsh, M. Kunz and A.R. Liddle, arXiv:0711.1842 [astro-ph].
- [50] A. Achúcarro and R. de Putter, Phys. Rev. **D74**, 121701 (2006).
- [51] M.G. Jackson, N.T. Jones and J. Polchinski, JHEP **10**, 013 (2005).
- [52] S. Borsanyi and M. Hindmarsh, arXiv:0712.0300 [hep-ph].
- [53] F. Dubath, J. Polchinski and J.V. Rocha, arXiv:astro-ph/0711.0994.
- [54] X. Siemens, X. Martin and K.D. Olum, Nucl. Phys. **B595**, 402 (2001).